

Outflowing Diffuse Gas in the Active Galactic Nucleus of NGC 1068

T. R. Geballe and R. E. Mason¹

T. Oka²

Received _____; accepted _____

¹Gemini Observatory, 670 N. A'ohoku Place, Hilo, HI, 96720, USA

²Department of Astronomy and Astrophysics and Department of Chemistry, The Enrico Fermi Institute, University of Chicago, 5735 South Ellis Avenue, Chicago, IL 60637, USA

ABSTRACT

Spectra of the archetypal Type II Seyfert galaxy NGC 1068 in a narrow wavelength interval near $3.7 \mu\text{m}$ have revealed a weak absorption feature due to two lines of the molecular ion H_3^+ . The observed wavelength of the feature corresponds to velocity of -70 km s^{-1} relative to the systemic velocity of the galaxy, implying an outward flow from the nucleus along the line of sight. The absorption by H_3^+ along with the previously known broad hydrocarbon absorption at $3.4 \mu\text{m}$ probably are formed in diffuse gas that is in close proximity to the continuum source, i.e. within a few tens of parsecs of the central engine. Based on that conclusion and the measured H_3^+ absorption velocity and with the assumption of a spherically symmetric wind we estimate a rate of mass outflow from the AGN of $\sim 1 \text{ M}_\odot \text{ yr}^{-1}$.

Subject headings: galaxies: active – galaxies: Seyfert – galaxies: ISM – ISM: molecules

1. Introduction

Active galactic nuclei (AGNs) contain a number of components on various spatial scales: the accretion disk, broad-line region (BLR), torus, narrow-line region (NLR), etc. Rather than being the static, well-defined structures that these terms may imply, in reality they are probably complex, dynamic, and in close interaction with each other and with the AGN’s host galaxy. For example, spectroscopy of the NLR in some high-redshift quasars suggests that an AGN-driven outflow can suppress star formation in the host galaxy (Cano-Díaz et al. 2012). On much smaller scales, the dusty torus of the AGN unified model may be produced by gas flowing towards the AGN and play a central role in regulating accretion (Hopkins et al. 2012). Conversely, others have suggested that the torus originates in gas flowing out from the AGN (Elitzur & Schlosman 2006), or is formed by the interplay between inflow and outflow (Wada 2012). Understanding the motions of gas in AGNs may therefore reveal clues about the way in which AGN and their surroundings interact with each other and evolve over time.

One might expect that where there is a dusty torus there are molecules and that therefore, for a heavily obscured Type II AGN, infrared spectroscopy of the central source would reveal absorption lines from molecules in or associated with the obscuring toroid, thereby probing the kinematics of the material on the line of sight to and close to the central engine. The most extensive such spectroscopy to date has been of the archetypal Seyfert II galaxy, NGC 1068. However, those observations, at a variety of spectral resolutions (Lutz et al. 2004; Mason et al. 2006; Geballe et al. 2009), failed to detect lines of what should be the strongest infrared molecular band, the fundamental vibration-rotation band of carbon monoxide (CO) near $5 \mu\text{m}$. Geballe et al. (2009) concluded that the gaseous environment directly in front of NGC 1068’s AGN, as viewed at mid-infrared wavelengths, is more similar to diffuse clouds, which have densities of $10\text{-}300 \text{ cm}^{-3}$, than dense clouds,

which have higher densities. This conclusion was based not only on the absence of CO, but also on the presence of the 3.4- μm hydrocarbon absorption feature in NGC 1068 (Bridger, Wright, & Geballe 1994), which is not found in Galactic dense clouds and is a reliable signature of a diffuse cloud environment. In Galactic diffuse clouds typically half of the hydrogen is in molecular form (H_2), but only about one percent of the carbon is in CO. A similar percentage of carbon in CO on the sightline to NGC 1068 would be consistent with its non-detection there (Geballe et al. 2009).

Unlike emission spectroscopy, absorption spectroscopy samples material only directly on the line of sight to a background continuum source. At 3–5 μm the bright central source of NGC 1068 has an unresolved or marginally resolved core of linear dimension less than $0''.05$ (3.5 pc at the 14.4 Mpc distance to NGC 1068) and a complex surrounding morphology of characteristic dimension $\sim 1''$ (Gratadour et al. 2006). When observed at 3–5 μm in good seeing on large telescopes without the benefit of adaptive optics the nuclear source has an effective full width at half maximum (FWHM) of $\sim 0''.3$ (20 pc) in the N-S direction (Geballe et al. 2009). The galactic disk of NGC 1068 is inclined at 40° such that the near side of the minor axis of the galaxy lies to southeast (de Vaucouleurs et al. 1991, see also de Vaucouleurs 1958); thus the sightline to the AGN passes through only a small portion of the galaxy within the nuclear region, and does not pass through the disk of the galaxy.

Combined knowledge of the detailed morphology and kinematics of the gas in the vicinity of an AGN is important for understanding the infall and/or outflow close to the central engine. For NGC 1068, García-Burillo et al. (2014) have used the Atacama Large Millimeter Array (ALMA) to observe the molecular gas and dust in this region, finding that the bulk of each is located in a circumnuclear disk (CND) of outer radius ~ 200 pc whose center is offset by a few tens of parsecs from the position of the AGN. From the profiles and intensity ratios of some of the submillimeter lines in the CND they have identified

the kinematic signature of a massive outflow, with a rate of many tens of solar masses per year. They identify the gas responsible for this signature as disk material being entrained by the ionized wind from the AGN. Closer to the AGN, on scales of 3–30 pc from the center, Muller Sanchez et al. (2009) have found that the kinematics and morphology of the $2.12 \mu\text{m}$ H_2 line emission indicate linear streamers of gas are fueling the nucleus, and thus presumably the outflow. They interpret some of this gas as being situated on the near side of the nucleus. A contrasting interpretation of the H_2 line emission is given by Barbosa et al. (2014), based on their velocity channel maps in the inner few hundred parsecs, obtained at a resolution of 8 pc. They find that their H_2 data are consistent with a radially expanding ring located in the plane of the galaxy. Regardless of the interpretation it is likely that the H_2 line emission arises in a small fraction of the molecular gas that is at high temperature immediately following shock-excitation or perhaps X-ray heating, and whose motions are not necessarily representative of the kinematics of the neutral nuclear gas as a whole.

The CND observed by García-Burillo et al. (2014) overlaps the AGN on the sky, so it is important to know whether it passes in front of, behind, or through the AGN. The nucleus of NGC 1068 is distinguished by a prominent bicone of ionized gas at a position angle of $\sim 10^\circ$, extending several arc seconds on either side of the center. The ionization cone extending NNE from the AGN is much more prominent at optical wavelengths than the southern cone. Both that and the blue-shifts of the emission lines observed in it indicates that the NNE cone is tilted toward the sun. The plane of the CND is expected to be roughly perpendicular to the bicone. If so then the CND lies largely or entirely behind the AGN where they overlap on the sky. Nevertheless, in view of the huge quantity of molecular gas and dust that are present in the CND as well as the asymmetric location of the CND with respect to the central engine it remains surprising that until now no molecular absorption lines had been seen on the line of sight to the AGN.

Clearly, an observation of absorbing gas on the line of sight to the AGN could provide important additional information about gas motions close to the central engine. Because the search for absorption lines of CO has been unsuccessful, an alternative infrared probe of the foreground gas column is needed. One possible candidate species is H_3^+ . Although it is obviously an ion, H_3^+ is created by the reaction $\text{H}_2 + \text{H}_2^+ \rightarrow \text{H}_3^+ + \text{H}$ and resides in largely neutral and at least partially molecular gas. Vibration-rotation lines of H_3^+ , although generally weak, are readily detectable not only in dense clouds (Geballe & Oka 1996), but also in numerous Galactic diffuse clouds (McCall et al. 2002; Indriolo et al. 2007), including e.g. Cygnus OB2 No. 12 (Geballe et al. 1999), whose 3.4- μm feature is less than half the strength of that toward NGC 1068 (Whittet et al. 1997; Geballe et al. 2009). Unless the lines of H_3^+ are greatly broadened toward NGC 1068 one would expect to detect them on the line of sight to the AGN. The close pair of vibration-rotation lines (1-0 $R(1,1)^u$ and 1-0 $R(1,0)$), at rest wavelengths of 3.66808 μm and 3.66852 μm , respectively, which arise from the lowest levels of para and ortho H_3^+ , are the best candidates for detection. In both diffuse and dense clouds in the Galactic plane these are the only two levels that are appreciably populated and the doublet is the strongest H_3^+ absorption feature.

2. Observations and Data Reduction

L -band spectra of NGC 1068 were obtained at the Frederick C. Gillett Gemini North Telescope on UT 2011 July 24 and October 11 and on UT 2014 November 28 and December 3, for programs GN-2011B-Q-53 and GN-2014B-Q-57, respectively. Both sets of observations used the Gemini North Infrared Spectrograph (GNIRS), but in different configurations. The 2011 spectra were obtained using the 111 l/mm grating, short focal length camera and the 0.45 " wide slit and covered 3.49-3.79 μm . The 2014 spectra were obtained through the same slit, but used the long focal length camera and the 111 l/mm

grating, which covered 3.64-3.74 μm and were heavily oversampled in wavelength. In each case the resolution at the wavelength of the sought after H_3^+ lines was 0.00082 μm (70 km s^{-1}). The observations were obtained in the standard stare/nod-along-slit mode, with a nod of $\pm 3''$. The slit was oriented along the axis of the bicone at position angle 15° (E of N). The total exposure times were 64 minutes in 2011 and 120 minutes in 2014. Early type telluric standard stars were observed at closely similar air masses to NGC 1068 either before or after each set of observations. The measurements were made in photometric or near photometric conditions and in good seeing.

The initial stage of data reduction included flat-fielding, spike removal, extraction of spectra over $0''.75$ long regions of the slit, wavelength calibration (using telluric lines and accurate to 0.0001 μm , corresponding to 10 km s^{-1}), and ratioing by the spectra of the telluric standards. Normalized ratioed spectra were then shifted to compensate for differences in the earth's orbital motion relative to the coordinates of NGC 1068 on the different observing dates, and then combined to produce one spectrum for each of the two programs. The continuum of each spectrum had slight curvature, which we suspect is an instrumental effect due to differences in the distribution of light from NGC 1068 and the standard stars and different positioning of them in the slit; to remove it and obtain flat spectra each spectrum was divided by a spline fit to its continuum. The resultant spectra were then resampled on a common wavelength scale and coadded with equal weighting (as their noise levels are similar) in the narrow wavelength interval encompassing the expected wavelength of the H_3^+ doublet, near 3.682 μm . Strong telluric absorption lines are present on either side of this wavelength, but the interval 3.675-3.686 μm , where the redshifted H_3^+ doublet is expected to fall, is devoid of significant interference. The spectra from semesters 2011B and 2014B and the final combined spectrum are shown in Fig. 1.

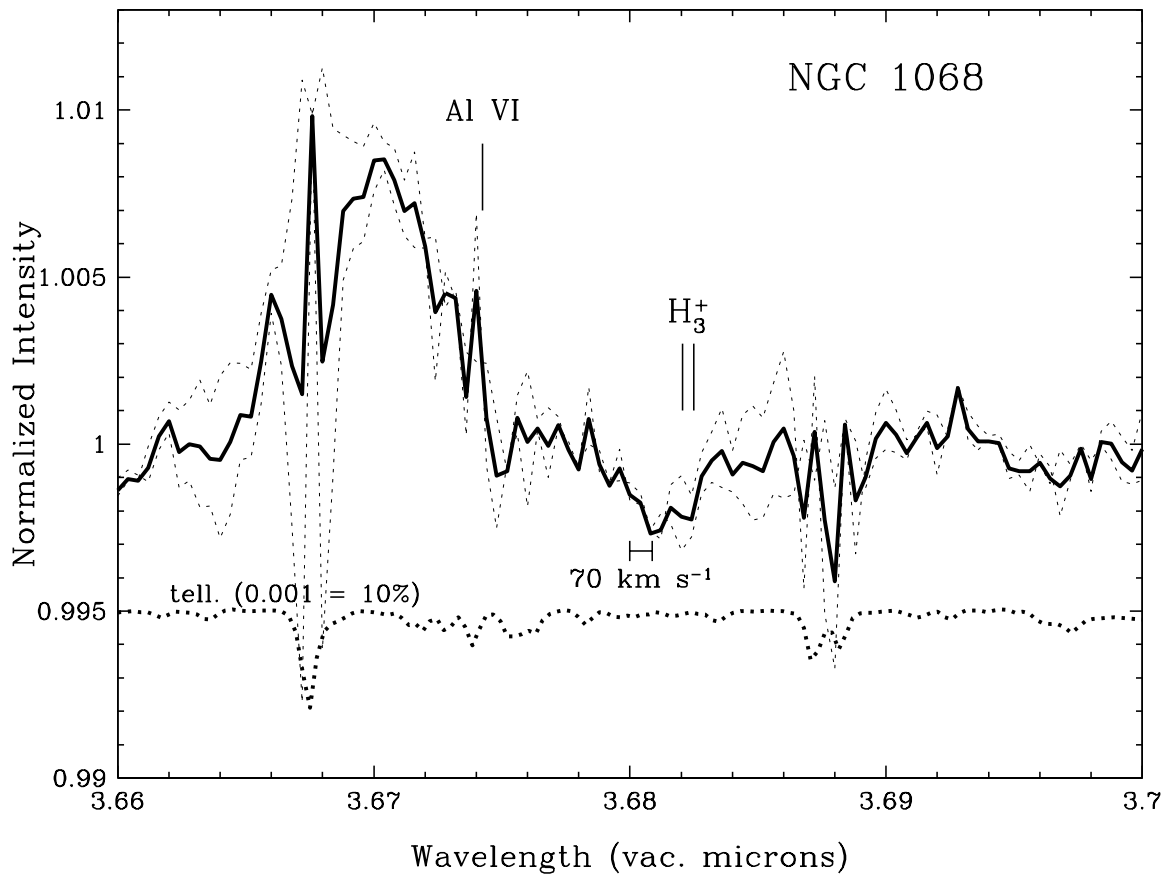


Fig. 1.— Spectrum of the infrared nuclear source in NGC 1068 near the H_3^+ para and ortho line pair, at a resolution of 70 km s^{-1} . The spectra from 2011 and 2014 (light dotted lines) and the combined spectrum (dark line) are shown, as is a 100 times scaled down spectrum of the atmospheric transmission (dark dotted line). The wavelengths of the H_3^+ lines and of the adjacent [Al VI] coronal line are indicated for a systemic heliocentric velocity of 1142 km s^{-1} (see text).

3. Results

The combined spectrum in Fig. 1 shows a detection of a very weak absorption feature with its centroid at $3.6815 \mu\text{m}$, which we identify as the blended pair of lines of para and ortho H_3^+ mentioned above. A coronal emission line of $[\text{Al VI}]$, previously reported by Geballe et al. (2009) is also present in the spectrum. Based on the fluctuations in the adjacent continuum in the combined spectrum the detection of the H_3^+ feature is at the 6σ confidence level. However, the differences in the 2011 and 2014 spectra on the long wavelength portion of the continuum suggest that the true confidence level is not quite that high. In estimating the continuum and the noise (the latter based on point-to-point fluctuations in the spectrum) we ignored the spectral intervals near the telluric lines at $3.674 \mu\text{m}$ and $3.688 \mu\text{m}$, as the noise levels there (which are dominated by fluctuations in the sky background) are significantly higher than elsewhere.

Assuming a systemic heliocentric velocity of 1142 km s^{-1} (from the H I Parkes All Sky Survey, as reported in the NASA/IPAC Extragalactic Database), the centroid of the absorption is blue-shifted by approximately 70 km s^{-1} from the systemic velocity of NGC 1068, indicating that the gas associated with the H_3^+ is flowing outward from the nucleus. The feature has a measured equivalent width of $5.2 \pm 0.8 \times 10^{-6} \mu\text{m}$ and an observed FWHM of $\sim 150 \text{ km s}^{-1}$. Assuming that the two lines, which are separated by 36 km s^{-1} , contribute equally to the feature, as they approximately do in Galactic diffuse clouds, the combined column density in the (1,1) and (1,0) levels is $7 \times 10^{14} \text{ cm}^{-2}$ and the intrinsic FWHM of a single absorption line is approximately 100 km s^{-1} . That width is considerably narrower than the more highly blue-shifted $[\text{Al VI}]$ line in Fig. 1. Geballe et al. (2009) found that the peak intensity of the infrared coronal lines occurs a few tenths of an arc-second to the north of the infrared continuum peak. The present data also show that separation. Clearly the gas responsible for the absorption by H_3^+ and the gas in

which the line emission by [Al VI] arises are in completely different locations and physical environments.

Other key lines of H_3^+ that could confirm the identification of the 3.6815- μm feature as due to H_3^+ and could provide constraints on the temperature and density of the material in which it originates are the $R(1,1)^l$ and $R(3,3)^l$ lines at 3.71548 μm and 3.53366 μm , respectively. Unfortunately each of these lines is likely to be weaker than the unresolved doublet and each is shifted into a wavelength interval where strong telluric absorption lines are present. Despite the lack of confirmatory evidence we are confident in the identification of H_3^+ , as (1) there are no other likely identifications for the feature and (2) the line pair was expected to be readily detected. For example, if the equivalent width of the doublet in NGC 1068 scaled as the ratio of equivalent widths of the observed 3.4 μm and doublet in the Galactic center (see Fig. 2), the equivalent width of the doublet in NGC 1068 would be 3×10^{-5} μm , six times greater than that observed. The surprising weakness of the doublet in NGC 1068 is discussed below.

4. Discussion

4.1. Extinctions to and Locations of Continuum and Absorption Feature

L-band spectra of NGC 1068 have yielded two absorption features, a prominent 3.4 μm feature generally ascribed to aliphatic hydrocarbons, and a weak absorption due to a pair of closely spaced lines of H_3^+ . Understanding where on the line of sight these absorptions occur requires first of all knowledge of the location of the source or sources of the infrared continuum. The adaptive optics images of Gratadour et al. (2006) show that within the portions of the slit from which the spectra of these features were extracted, by Geballe et al. (2009) for 3.4 μm feature ($0''.2 \times 1''.0$) and by us for the H_3^+ feature ($0''.45 \times 0''.75$), the

continuum is produced by a high surface brightness core and a complex morphology of more extended and lower surface brightness regions with the two being roughly comparable in total signal.

Whatever the explanation for the L -band morphology; the likelihood is that the continuum is thermal emission from clouds containing hot dust (e.g., Gratadour et al. 2006), presumably heated by the central engine. If so, the continuum probably arises in the vicinity of each $\tau=1$ (in the L band) surface in this complex region; in other words at distances of a few parsecs to a few tens of parsecs from the engine. One can also estimate the mean optical depth to the L -band continuum from the depth of the $3.4\ \mu\text{m}$ feature, assuming the relationship between the depth of the feature and the optical extinction in Galactic diffuse clouds (Godard et al. 2012) holds for NGC 1068, where the optical depth of the feature is 0.08 (Geballe et al. 2009). This assumption yields a visual extinction of ~ 21 mag, which, for normal extinction curves (e.g., extinction proportional to $\lambda^{-1.7}$) implies an L -band optical depth close to unity. The near equality of the optical depths derived in these different ways is either a coincidence or, as we suspect, an indication that the dust producing the L -band continuum and the carrier of the $3.4\ \mu\text{m}$ absorption (and by association the absorbing H_3^+) are physically close to one another, placing the absorbing material within a few tens of parsecs of the central engine. This proximity is not surprising in view of the orientation of the disk of the galaxy, as discussed earlier.

4.2. Low H_3^+ Equivalent Width

Figure 2 is a plot of the equivalent width of that portion of the H_3^+ line pair arising in diffuse gas versus the equivalent width of the $3.4\text{-}\mu\text{m}$ absorption feature, for four sources: the Galactic plane source Cyg OB2 No. 12, the Galactic center’s tight cluster of four sources known as GCS 3 (of which the brightest component is GCS 3-2), the ultraluminous

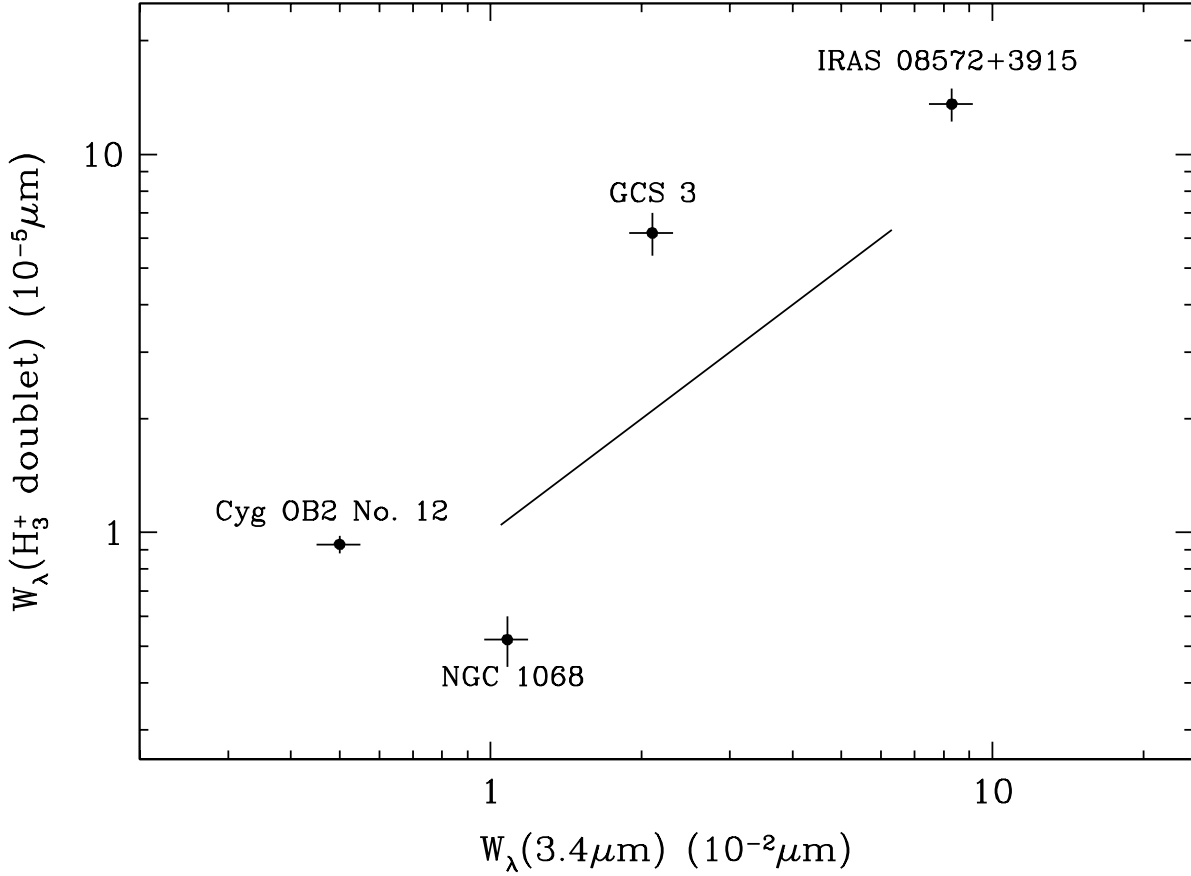


Fig. 2.— Equivalent width of that portion of the absorption by the H_3^+ para-ortho line pair ascribed to diffuse gas vs. equivalent width of the $3.4\mu\text{m}$ feature, for Cygnus OB2 No. 12, the Galactic center Quintuplet source(s) GCS 3, the ultraluminous infrared galaxy (ULIRG) IRAS 08572+3915, and NGC 1068. Error bars are $\pm 1\sigma$. The diagonal line is a one-to-one relationship between the two equivalent widths. The equivalent width of the H_3^+ feature in GCS 3 is based on the measurement toward GCS 3-2. In all but GCS3-2 the absorption by H_3^+ is assumed to be formed entirely in diffuse gas. In GCS 3-2 the contribution by H_3^+ in dense clouds has been subtracted. See text for details.

infrared galaxy (ULIRG) IRAS 08572+3915, and NGC 1068. The H_3^+ equivalent widths for the first three sources are obtained from data or figures in Geballe et al. (1999), Oka et al. (2005), and Geballe et al. (2006), respectively. The equivalent widths of the 3.4- μm feature were measured from spectra in Sandford et al. (1991), Chiar et al. (2000), Geballe et al. (2006), and Mason et al. (2006), respectively. For Cyg OB2 No. 12, IRAS 08572+3915, and NGC 1068 either all of the H_3^+ or the vast majority of it is known or thought to be in diffuse gas; (see Geballe et al. 2006, for the argument pertaining to IRAS 08572+3915). In the case of GCS 3-2, however, the sightline passes through both diffuse and dense interstellar gas. Oka et al. (2005) have determined the column densities in each environment. A further complication is that the lines are Doppler broadened so that the pair is observed as a blend. However, Oka et al. (2005) also estimated the populations in the (1,1) and (1,0) levels, allowing the equivalent width of the blended pair of lines, which absorb from those levels, to be determined using the formula in Geballe & Oka (1996) relating level column density to line equivalent width.

If the bulk of the H_3^+ is in the lowest para and lowest ortho levels, as is generally the case, then the equivalent width of the line pair represents the total column density of H_3^+ . One then would naively expect that the equivalent widths in Fig. 2 would scale with one another. NGC 1068 clearly deviates the most from following that trend; the discrepancy is roughly a factor of six. This suggests either that an unusually low fraction of its total H_3^+ column density resides in its two lowest energy levels or that it has a highly enhanced abundance of the carrier of the 3.4- μm absorption feature, or both. There are several possible explanations for this anomaly, which we now list and briefly discuss.

1. H_3^+ in other energy levels: For cold diffuse gas such as that in front of Cygnus OB2 No. 12 the (1,1) and (1,0) levels are the only ones that are significantly populated. In the Galactic center, where the density of the diffuse gas containing the H_3^+ is $\sim 100 \text{ cm}^{-3}$

and the gas temperature is ~ 250 K the metastable (3,3) level contains about 23% of the H_3^+ and altogether all of the levels higher than (1,1) and (1,0) contain about 30% of the H_3^+ (Oka et al. 2005). Thus the correction, which would move its data point upward by 30% in Fig. 2 is modest. In IRAS 08572+3915 the large column densities implied by the strong H_3^+ lines suggest that the H_3^+ is distributed along a column length of hundreds of parsecs (Geballe et al. 2006). Much of this extended region is likely to be at temperatures that are no higher than those in the Galactic center, and thus we believe that the upward correction is also small.

If the H_3^+ observed toward NGC 1068 is in gas physically associated with the continuum source, as we suspect, its temperature could be higher. Gratadour et al. (2006) suggest dust temperatures of ~ 600 K for the dust emitting in the L band. Alloin & Marco (1997), observing at K , L , and M , found a mean dust temperature of 750 K for the central ~ 1 -arc second region. Jaffe et al. (2004), observing near $10 \mu\text{m}$, find a 320 K in the central few parsecs, as do others (Mason et al. 2006; Poncelet, Sol, & Perrin 2008). Thus a significant portion of the absorbing column may have a higher proportion of H_3^+ in higher levels than the Galactic center. However, due to the wide spacing of rotation energy levels in the ground vibrational state (e.g., the $J=4$ levels have excitation energies $>1,000$ K) as well as depopulation via spontaneous decay of many of the excited rotational states at the low densities of diffuse gas (Oka & Epp 2004), we expect the correction to be less than a factor of two. Thus we do not think that large populations in higher energy levels can explain the discrepant data point in Fig. 2.

2. Higher gas density and shorter column length: In diffuse gas the density of H_3^+ does not track the total number density of the gas in which it is located, but is a constant whose value depends on the rate of cosmic ray ionization of H_2 and the rate of dissociative recombination of H_3^+ on electrons (Geballe et al. 1999). Thus the column

density of H_3^+ scales with column length rather than with gas column density. If the mean density of the diffuse environment in front of the AGN in NGC 1068 is higher than in typical diffuse clouds, the column density of H_3^+ there will be lower relative to other species. Likewise, a larger than normal density of free electrons, which is the principal destroyer of H_3^+ in diffuse gas, would result in a lower steady state density of H_3^+ and also in a lower column density.

3. Low fractional abundance of H_2 : As discussed in Section 2.3.2 of Oka (2013) the abundance of H_3^+ is approximately proportional to the square of the fractional abundance of molecular hydrogen, $f(\text{H}_2) = 2n(\text{H}_2)/[n(\text{H}) + 2n(\text{H}_2)]$. A value of $f(\text{H}_2)$ that is smaller by a factor of 2.5 than in typical Galactic diffuse clouds could explain the low abundance of H_3^+ . In NGC 1068 the abundance of H_2 might well be lower than normal in the hostile environment close to the AGN.

4. High abundance of carbon and/or the carrier of the 3.4- μm feature:

The 3.4- μm feature is generally attributed to C-H stretching vibrations in aliphatic hydrocarbons. As such the strength of the feature is sensitive to the carbon abundance and is likely to be greater toward the centers of galaxies, paralleling expected or observed increases in metallicity. In diffuse clouds, where most of the carbon is singly ionized, a higher abundance of carbon also results in a higher electron density and a lower steady state abundance of H_3^+ . Judging from Fig. 2, if these effects alone were to account for the discrepancy the carbon abundance in the nucleus of NGC 1068 would need to be several times higher than in the nuclear regions of IRAS 08572+3915 or the Galactic center. We have found no observations of NGC 1068 in the literature that are pertinent to this issue.

To summarize this subsection, there are several possible explanations for the unusually low value of the ratio of equivalent widths of the H_3^+ and 3.4- μm absorption features on the

sightline to the AGN in NGC 1068. One, some, or all of them could contribute and we are unable to select a likely dominant contributor.

4.3. Outflow and Mass Loss

The observation of a blue-shifted H_3^+ absorption feature at $3.7 \mu\text{m}$ indicates that on the line of sight to the nucleus, and thus quite far removed from the axis of the ionization bicone, there exists outflowing gas located close to where L -band continuum is formed, at a distance of possibly only a few parsecs or a few tens of parsecs from the central engine. The relationship of this outflow to the apparently much more powerful flow largely within the ionization bicone, which probably originates much closer to the central engine, is unclear.

Based on the H_3^+ absorption feature, a very crude estimate of the rate of mass outflow can be derived. We based our estimate on (1) the H_3^+ being in the same diffuse interstellar environment that produces the $3.4\text{-}\mu\text{m}$ hydrocarbon feature and (2) our interpretation that the similar values of the likely optical depth to the source of the L -band continuum and the optical depth estimated from the hydrocarbon feature mean that the diffuse gas is in proximity to the continuum sources rather than at a great distance from them. Using a diffuse cloud gas density of 100 cm^{-3} and a mean distance of the flow at that density of 20 pc, together with the highly dubious assumption of isotropy of the outflow, we obtain an outflow rate of $1 M_\odot \text{ yr}^{-1}$. The rate is proportional to the square of the assumed mean distance, which together with the assumption of spherical symmetry have high uncertainties. Other contributors to the uncertainty are the outflow velocity, which depends on the choice of systemic velocity, and the mean density of the absorbing diffuse gas. We regard the above value of mass outflow rate as an order of magnitude estimate only.

If our estimate of 20 pc for the location of the diffuse gas is roughly correct then the

outflow observed in H_3^+ exists on distance scales smaller than those probed by the ALMA millimeter and submillimeter spectroscopy of the CND. Based on the analysis of molecular line profiles at distances of 100-200 pc from the center García-Burillo et al. (2014) recently deduced the existence of an outflow originating in the AGN with a mass loss rate 1-2 orders of magnitude greater than we derive from the blueshifted H_3^+ absorption. They also measure outflow velocities of up to a few hundred km s^{-1} , considerably higher than seen in H_3^+ . Barbosa et al. (2014) also observe higher velocities, but derive a mass loss rate, based on the kinematics of the ionized gas similar to our rough estimate for the diffuse molecular gas. Unlike the outward flowing H_3^+ observed by us, which is far from being along the axis of the bicone, the outflowing gas that both of these groups have observed is within or at least much closer to the bicone. Much higher velocities, up to $1,000 \text{ km s}^{-1}$, also are observed from the bicone in numerous optical and infrared emission lines (e.g., Crenshaw & Kraemer 2000; Das et al. 2006; Poncelet, Sol, & Perrin 2008).

The differences in mass loss rates derived here and by García-Burillo et al. (2014) thus may indicate large anisotropies in the outflow, but also could easily be due to time variability both in intensity and in the direction of the outflow. Approximately 10^5 years are required for gas moving at $1,000 \text{ km s}^{-1}$ to travel 100 pc (the distance from the central engine to the inner edge of the CND). On the other hand, it seems reasonable that although the outflow is primarily within the bicone, it has an associated and much weaker component in other directions. That portion of the flow would be more shielded from the strong ultraviolet field present in the bicone and would allow gas that on the line of sight to become or to remain partially molecular, although quite close to the AGN.

5. Conclusions

We have detected a weak absorption by blue-shifted H_3^+ on the line of sight to the central bright infrared continuum source of the type II Seyfert galaxy NGC 1068. This is only the second detection of H_3^+ in an extragalactic object. Surprisingly H_3^+ is the only interstellar molecule in NGC 1068 that has been detected in absorption toward its AGN. Its presence is consistent with the existence in front of the AGN of a significant column density of diffuse gas, previously known to be present by a prominent $3.4\text{-}\mu\text{m}$ hydrocarbon feature, and also from the absence of absorption in the fundamental band of carbon monoxide. We tentatively conclude that the diffuse gas is situated within a few tens of parsecs of the central engine and estimate an (isotropic) mass outflow rate of $1\text{ M}_\odot\text{ yr}^{-1}$ with an uncertainty of an order of magnitude. This rate is lower by 1-2 orders of magnitude than the rate recently deduced by García-Burillo et al. (2014) from ALMA observations of line profiles in the 100-200 pc radius CND, but is roughly consistent with the rate derived by Barbosa et al. (2014). The H_3^+ absorption is considerably weaker than expected from the strength of the $3.4\text{-}\mu\text{m}$ feature. This could be explained by the gas being at a higher temperature, by the fraction of hydrogen in molecular form being 2-3 times lower than typical for diffuse clouds, by an unusually high abundance of carbon in the nucleus, or by the diffuse gas in which the absorption takes place being considerably higher density than standard Galactic diffuse clouds in which H_3^+ has previously been detected.

Acknowledgements

This paper is based on observations obtained at the Gemini Observatory, which is operated by the Association of Universities for Research in Astronomy, Inc., under a cooperative agreement with the NSF on behalf of the Gemini partnership: the National Science Foundation (United States), the National Research Council (Canada), CONICYT

(Chile), the Australian Research Council (Australia), Ministério da Ciência, Tecnologia e Inovação (Brazil) and Ministerio de Ciencia, Tecnología e Innovación Productiva (Argentina).

REFERENCES

- Alloin, D. & Marco, O. 1997, *ApSS*, 248,237
- Antonucci, R. 1993, *ARAA*, 31, 473
- Barbosa, F. K. B., Storchi-Bergmann, T., McGregor, P., Vale, T. B., & Riffel, A. R. 2014, *MNRAS*, 445, 2353
- Bridger, A., Wright, G. S., & Geballe, T.R. 1994, in "Infrared Spectroscopy With Arrays: The Next Generation," ed. I.S. McLean, Kluwer (Dordrecht), 537
- Cano-Díaz, M. Maiolino, R., Marconi, A., Netzer, H., O., Shemmer, O., & Cresci, G. 2012, *A&A*, 537, L8
- Chiar, J., Tielens, A. G. G. M., Whittet, D. C. B., Schutte, W. A., Boogert, A. C. A., Lutz, D., van Dishoeck, E., & Bernstein, M. P. 2000, *ApJ*, 537, 749
- Crenshaw, D.M. & Kraemer, S. B. 2000, *ApJ*, 532, L101
- Das, V., Crenshaw, D. M., Kraemer, S. B., & Deo, R. P. 2006, *AJ*, 132, 620
- García-Burillo, S., Combes, F., Usero, A., et al. 2014, *A&A*, 567, A125
- Geballe, T. R. & Oka, T. 1996, *Nature*, 384, 334
- Geballe, T. R., McCall, B. J., Oka, T., & Hinkle, K.H. 1999, *ApJ*, 510, 251
- Geballe, T. R., Goto, M., Usuda, T., Oka, T., & McCall, B. J. 2006, *ApJ*, 644, 907
- Geballe, T. R., Mason, R. E., Rodriguez-Ardila, A., Axon, D. J. 2009, *ApJ*, 701, 1710
- Godard, M., Geballe, T. R., Dartois, E., & Muñoz Caro, G. M. 2012, *A&A*, 537, A27
- Gratadour, D., Rouan, D., Mugnier, L. M., et al. 2006, *A&A*, 446, 813

- Hopkins, P. F., Hayward, C. C., Narayanan, D., & Hernquist, L. 2012, MNRAS, 420, 320
- Jaffe, W., Meisenheimer, K., Röttgering, H. J. A, et al. 2004, Nature, 429, 47
- Lutz, D., Sturm, E., Genzel, R., Spoon, H. W. W., & Stacey, G. J. 2004, A&A, 426, L5
- Indriolo, N., Geballe, T. R., Oka, T., & McCall, B. J. 2007, ApJ, 671, 1736
- Mason, R. E., Geballe, T. R., Packham, C., et al. 2006, ApJ, 640, 612
- McCall, B. J., Hinkle, K. H., Geballe, T. R. et al. 2002, ApJ, 567, 391
- Muller Sanchez, F., Davies, R. I., Genzel, R., et al. 2009, ApJ, 691, 749
- Oka, T. & Epp, E. 2004, ApJ, 613, 349
- Oka, T., Geballe, T. R., Goto, M., Usuda, T., & McCall, B. J. 2005, ApJ, 632, 882
- Oka, T., 2013, Chem. Rev., 113, 8738
- Poncelet, A., Sol, H, & Perrin, G. 2008, A&A, 481, 305
- Sandford, S. A., Allamandola, L. J., Tielens, A. G.G. M., Sellgren, K., Tapia, M., & Pendleton, Y. 1991, ApJ, 371, 607
- de Vaucouleurs, G. 1958, ApJ, 127, 487
- de Vaucouleurs, G. et al. 1991. Third Reference Catalogue of Bright Galaxies. Springer-Verlag, New York
- Whittet, D. C.B., Boogert, A. C. A., Gerakines, P. A., et al. 1997, ApJ, 490, 729
- Wolniewicz, L., Simbotin, I., & Dalgarno, A. 1998, ApJS, 115, 293